

Preparation and magnetic hardening of low Ti content $(Sm,Zr)(Fe,Co,Ti)_{12}$ magnets by rapid solidification non-equilibrium method

Xing-Feng Zhang(张兴凤), Li-Bin Liu(刘立斌), Yu-Qing Li(李玉卿), Dong-Tao Zhang(张东涛), Wei-Qiang Liu(刘卫强), and Ming Yue(岳明)

Citation: Chin. Phys. B, 2024, 33 (**9**): 097503. DOI: 10.1088/1674-1056/ad58c4
Journal homepage: http://cpb.iphy.ac.cn; http://iopscience.iop.org/cpb

What follows is a list of articles you may be interested in

MHz cut-off frequency and permeability mechanism of iron-based soft magnetic composites

Xiao-Wei Jin(金校伟), Tong Li(李通), Hui-Gang Shi(史慧刚), and De-Sheng Xue(薛德胜)
Chin. Phys. B, 2024, 33 (**9**): 097501. DOI: 10.1088/1674-1056/ad57aa

Magnetic domain structures in ultrathin $Bi_2Te_3/CrTe_2$ heterostructures

Tirui Xia(夏体瑞), Xiaotian Yang(杨笑天), Yifan Zhang(张逸凡), Xinqi Liu(刘馨琪), Xinyu Cai(蔡新雨), Chang Liu(刘畅), Qi Yao(姚岐), Xufeng Kou(寇煦丰), and Wenbo Wang(王文波)
Chin. Phys. B, 2024, 33 (**8**): 087504. DOI: 10.1088/1674-1056/ad4a3a

Magnetic and magnetocaloric effect of $Er_{20}Ho_{20}Dy_{20}Cu_{20}Ni_{20}$ high-entropy metallic glass

Shi-Lin Yu(于世霖), Lu Tian(田路), Jun-Feng Wang(王俊峰), Xin-Guo Zhao(赵新国), Da Li(李达), Zhao-Jun Mo(莫兆军), and Bing Li(李昺)
Chin. Phys. B, 2024, 33 (**5**): 057502. DOI: 10.1088/1674-1056/ad1a94

Analytical solutions to the precession relaxation of magnetization with uniaxial anisotropy

Ze-Nan Zhang(张泽南), Zhen-Lin Jia(贾镇林), and De-Sheng Xue(薛德胜)
Chin. Phys. B, 2024, 33 (**4**): 047502. DOI: 10.1088/1674-1056/ad08a3

Enhanced resonance frequency in Co_2FeAl thin film with different thicknesses grown on flexible graphene substrate

Cai Zhou(周偲), Shaokang Yuan(袁少康), Dengyu Zhu(朱登玉), Yuming Bai(白宇明), Tao Wang(王韬), Fufu Liu(刘福福), Lulu Pan(潘禄禄), Cunfang Feng(冯存芳), Bohan Zhang(张博涵), Daping He(何大平), and Shengxiang Wang(汪胜祥)
Chin. Phys. B, 2024, 33 (**3**): 037506. DOI: 10.1088/1674-1056/acfafa

---

Preparation and magnetic hardening of low Ti content (Sm,Zr)(Fe,Co,Ti)$_{12}$ magnets by rapid solidification non-equilibrium method

Xing-Feng Zhang(张兴凤), Li-Bin Liu(刘立斌), Yu-Qing Li(李玉卿)[†],
Dong-Tao Zhang(张东涛), Wei-Qiang Liu(刘卫强), and Ming Yue(岳明)[‡]

College of Materials Science and Engineering, Key Laboratory of Advanced Functional Materials, Ministry of Education of China, Beijing University of Technology, Beijing 100124, *China*

(Received 1 March 2024; revised manuscript received 30 May 2024; accepted manuscript online 17 June 2024)

The Sm–Zr–Fe–Co–Ti quinary-alloys with ThMn$_{12}$ structure has attracted wide attention for ultra-high intrinsic magnetic properties, showing potentiality to be developed into rare-earth permanent magnets. The Ti element in alloys is crucial for phase stability and magnetic properties, and lower Ti content can increase intrinsic magnetic properties but reduce phase stability. In this study, the 1:12 single-phase melt-spun ribbons with low Ti content was successfully prepared using a rapid solidification non-equilibrium method for the $Sm_{1.1}Zr_{0.2}Fe_{9.2}Co_{2.3}Ti_{0.5}$ quinary-alloy. However, this non-equilibrium ribbon did not achieve good magnetic hardening due to the uneven microstructure and microstrain. Then, annealing was carried out to eliminate micro-strain and homogenize microstructure, therefore, remanence and coercivity were significantly improved even the precipitation of a small amount of α-Fe phase which were not conducive to coercivity. The remanence of 86.1 emu/g and coercivity of 151 kA/m was achieved when annealing at 850 °C for 45 min. After hot pressing, under the action of high temperature and pressure, a small portion of ThMn$_{12}$ phases in the magnet decompose into Sm-rich phases and α-Fe, while remanence of 4.02 kGs (1 Gs = 10^{-4} T), and coercivity of 1.12 kOe (1 Oe = 79.5775 A·m^{-1}) were still acquired. Our findings can provide reference for exploring practical permanent magnets made of 1:12 type quinary-alloys.

Keywords: magnetic materials, (Sm,Zr)(Fe,Co,Ti)$_{12}$ magnets, nanocrystalline magnet, microstructure

PACS: 75.50.Ww, 75.75.–C, 75.75.Cd **DOI:** 10.1088/1674-1056/ad58c4

1. Introduction

Rare earth permanent magnet materials are key raw materials for electric drive systems and are used in numerous military and commercial fields. Improving the magnetic properties of permanent magnet is the key to promoting the rapid development of corresponding application fields. At present, the most widely used rare earth permanent magnet (Nd–Fe–B) has a magnetic energy product close to its theoretical value,[1,2] and contains a large amount of strategic rare earth elements (approximately 30 wt%), resulting in high production costs. Therefore, developing new magnets[3–7] with low rare earth content[8,9] and excellent comprehensive performance is a top priority in the field of permanent magnet materials.

For 1:12 rare earth-iron compounds, high Fe element is beneficial for obtaining high saturation magnetization, and hexagonal structure with low symmetry is beneficial for obtaining high magneto-crystalline anisotropy. In addition, a low rare earth content can save rare earth resources. The thermodynamics of the $ReFe_{12}$ compound was unstable,[10] and phase-stable elements M of Ti, Cr, V, Mn, Mo, etc. were necessary to form $RFe_{12-x}M_x$ stable compound.[11–13] The Ti element as a excellent choice as a phase stable element. The Ti element was crucial for phase stability and intrinsic magnetic properties.[14–16] Reducing Ti can improve intrinsic magnetic performance, but phase stability decreased.[17] When the Ti content was lowered to $Sm_{0.8}Zr_{0.2}(Fe_{0.8}Co_{0.2})_{11.5}Ti_{0.5}$,[18] the equilibrium state method cannot form a 1:12 single-phase structure, but at this time, the intrinsic magnetic performance is very excellent, with a Curie temperature of 830 K, a saturation magnetization strength of 1.53 T, and a magnetic crystal anisotropy field of 8.4 T. Furthermore, the researchers[19–21] found that introducing T (Y, Gd, Zr, etc.) to replace some Sm, and Co to replace a portion of Fe, moderate Ti content can form a (Sm,T)(Fe,Co)$_{12-x}$Ti$_x$ quinary-alloy, further increasing T_c and $\mu_0 M_s$ to about 800 K, 1.5 T, respectively, and $\mu_0 H_a$ between 8 T and 11 T.[22] Thus, the T_c of the 1:12 phase alloy was more than 200 K higher than that of the $Nd_2Fe_{14}B$ compound.[23]

On the one hand, from the perspective of intrinsic magnetic properties, $SmFe_{12}$ alloys were a strong competitor for the new generation of permanent magnetic materials. Recently, many reports[24–30] revealed that it was difficult to obtain good magnetic properties, especially to achieve good magnetic hardening based on the 1:12-type quinary-alloy. Since the phase stability of the 1:12-type phase in the quinary-alloy was not enough to support the high sintering tempera-

[†]Corresponding author. E-mail: yqli@bjut.edu.cn
[‡]Corresponding author. E-mail: yueming@bjut.edu.cn

© 2024 Chinese Physical Society and IOP Publishing Ltd

ture, it is hard to prepare bulk magnet by using the powder metallurgy process as the sintered Nd–Fe–B magnet. On the other hand, the decrease of grain size and/or particle size, introduction of defects can lower the phase stability of the 1:12-type phase in quinary-alloys, which is also adverse to prepare noncrystalline magnet. In addition to the limitation of phase stability, other factors affecting the magnetic hardening have not been identified yet, therefore, it is necessary to explore the 1:12-type quinary-alloys.

Thus, in this article, the 1:12 single-phase melt-spun ribbons with low Ti content was successfully prepared using a rapid solidification non-equilibrium method for the $Sm_{1.1}Zr_{0.2}Fe_{9.2}Co_{2.3}Ti_{0.5}$ quinary-alloy. The suitable vacuum annealing process for the $(Sm,Zr)(Fe,Co,Ti)_{12}$ melt-spun ribbons was proposed. After annealing, the remanence and coercivity improved even appearance of soft magnetically phase, α-Fe. Thus, the coercivity improvement mechanism was studied based on the microstructure characterization. In addition, the bulk nanocrystalline magnet was prepared by 1:12-type quinary-alloys ribbons using the vacuum spark-plasma-sintering.

2. Experimental details

The nominal compositions of $Sm_{1.1}Zr_{0.2}Fe_{9.2}Co_{2.3}Ti_{0.5}$ alloys were prepared by vacuum melting, and 3-wt% Sm was added to compensate the burn-loss. The alloys were melt-spun into ribbons using a copper wheel with a roll surface velocity of 15 m/s–45 m/s. Subsequently, the ribbons were crushed into powders and placed into WC-Co mold with a diameter of 15 mm, and prepared by spark plasma sintering (SPS) at 650 °C under high stress ($\approx$ 550 MPa) to obtain hot-pressed (HP) magnets. For annealing, the ribbons were sealed into a quartz tube under an argon atmosphere and quenched in water. Two parameters of heat treatment were set during annealing with the annealing temperature of 800 °C–900 °C and the annealing time of 15 min–60 min. The crystal structure of the magnet was characterized by x-ray diffraction (XRD), and the grain size and strain were analyzed through XRD results using JADE software. The magnetic properties of samples were measured by vibrating sample magnetometer (VSM) with a maximum applied field of 3 T. The microstructure of samples was analyzed by scanning electron microscope (SEM) and transmission electron microscope (TEM). The mi both before and after annealing crostrain analysis is based on high-resolution TEM images, using open-source software strain.[31]

3. Results

It is mainly difficult to determine the amount of Sm, as the Sm burning loss is not stable during high-temperature melting and rapid quenching processes. Firstly, a nominal $Sm_{0.9}Zr_{0.1}Fe_{9.2}Co_{2.3}Ti_{0.5}$ alloy with a burning loss of 3% Sm was carried out, and the results (see Fig. S1 in supporting information) showed that a 1:12 single-phase could not be formed by melt-spun, and adjusting the wheel speed still could not eliminate the α-Fe. Therefore, the Sm content was increased to $Sm_{1.1}Zr_{0.2}Fe_{9.2}Co_{2.3}Ti_{0.5}$. For the ingots, 1:12, 1:7, and α-Fe phases can be found in the XRD patterns and SEM–BSE images, revealing that obtaining a single 1:12 phase alloy through melting was impossible even the Sm content was increased.

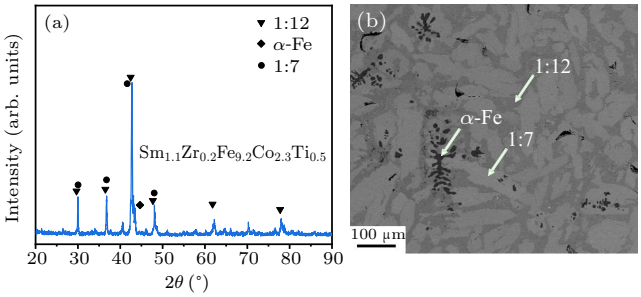


Fig. 1. XRD pattern (a) and SEM–BSE images (b) of $(Sm,Zr)(Fe,Co,Ti)_{12}$ alloy ingots.

Furthermore, by using the $Sm_{1.1}Zr_{0.2}Fe_{9.2}Co_{2.3}Ti_{0.5}$ ingots as raw materials, nanocrystalline powders was prepared by melt-spun (rapid-quenching) technology. Figure 2(a) showed the XRD patterns of ribbons obtained at different quenching-speeds (15 m/s to 45 m/s), showing a single-phase 1:12 phase with no obvious presence of a second phase. Due to the high volatility of Sm element during the smelting and high-temperature homogenizing heat treatment process, additional Sm (about 20%) was needed to be added to compensate.[30,31] In this paper, about 23% additional Sm was needed to obtain single 1:12 phase after melt-spun. However, even if a relatively pure 1:12 phase was obtained, magnetic hardening has not yet been achieved. As shown in Fig. 2(b), the hysteresis loops covered a very small area within the range of quenching-speeds of 15 m/s to 45 m/s. Therefore, the coercivity and remanence were relatively small as shown in Fig. 2(c). Tozman *et al.*[21] obtained an equilibrium state of $Sm_{0.8}Zr_{0.2}(Fe_{0.8}Co_{0.2})_{11.5}Ti_{0.5}$ quinary-alloy with 20% Sm burning loss through long-term annealing of ingots (annealing at 1100 °C for one week). At this time, the alloy was consisted of 1:12 phase (83 wt%) and α-Fe, indicating it is impossible to obtain a 1:12 single-phase. Our ingots (Fig. 1) without uniform annealing also exhibit complex phase structures, fail to obtain single phase. The ribbons prepared by the rapid quenching was non-equilibrium, which was the key to obtaining single-phase. Rapid solidification provided conditions for the formation of single-phase supersaturated solid solutions.

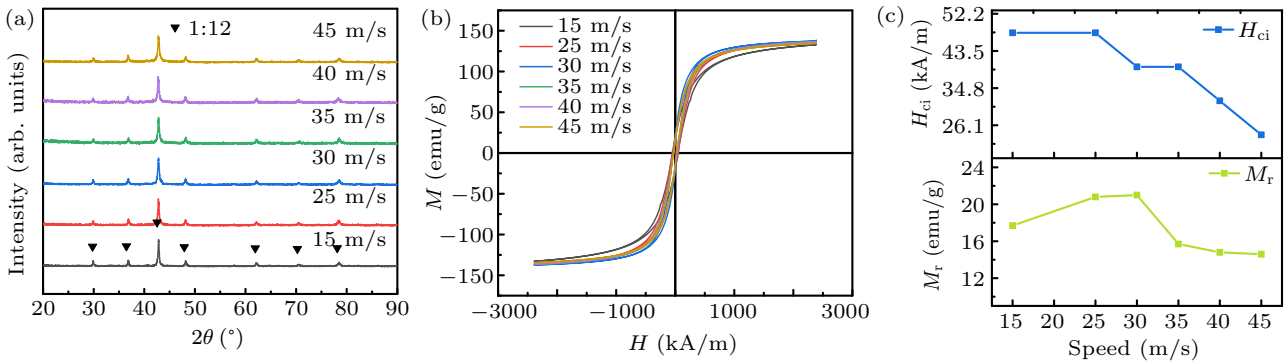


Fig. 2. XRD patterns (a), hysteresis loops (b), and magnetic properties (c) of the (Sm,Zr)(Fe,Co,Ti)$_{12}$ melt-spun ribbons with various quenching-speeds.

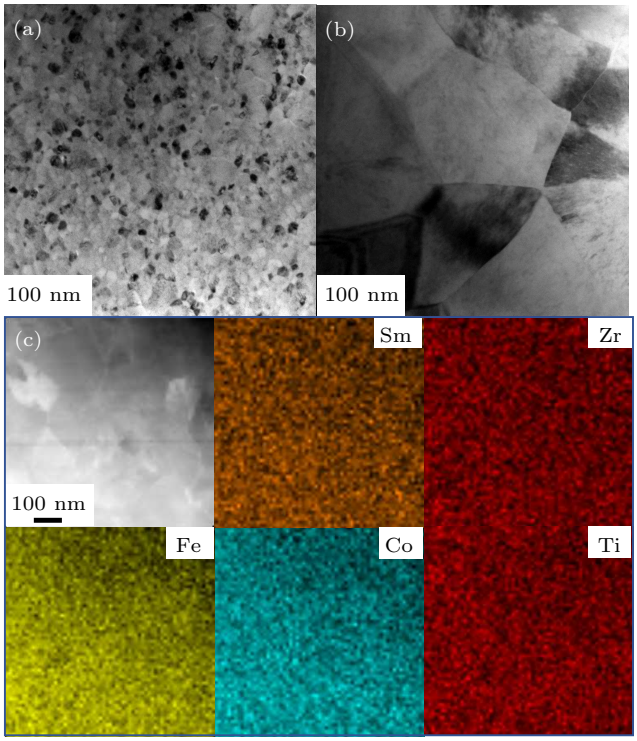


Fig. 3. TEM results of as-spun (Sm,Zr)(Fe,Co,Ti)$_{12}$ ribbons at a quenched speed of 30 m/s. Panels (a) and (b) are bright field images at different positions, panel (c) is the HAADF image and *in-situ* distribution maps of Sm, Zr, Fe, Co, Ti elements.

To understand the reasons for the low magnetic properties of the (Sm,Zr)(Fe,Co,Ti)$_{12}$ melt-spun ribbons, the microstructure characterization was carried out. In non-equilibrium supersaturated solid solutions, strain is easily introduced, and XRD analysis (marked by 30 m/s in Fig. 2(a)) showed a stress of 0.27% and the average grain size was 119 nm for the ribbons prepared with wheel speed of 30 m/s. Figure 3 shows the TEM results of (Sm,Zr)(Fe,Co,Ti)$_{12}$ melt-spun ribbons at a quenching-speed of 30 m/s. The non-uniform morphologies were observed, as shown in Figs. 3(a) and 3(b). Some regions (Fig. 3(a)) had fine nanocrystalline (20 nm–50 nm) structures, while others (Fig. 3(b)) had significantly coarser grain sizes (over 200 nm). Furthermore, the distribution of Sm, Zr, Fe, Co, and Ti was relatively uniform, and no obvious element segregation phenomenon was observed from element mapping (Fig. 3(c)).

Annealing is an effective way to improve the magnetic performance of magnetic ribbons. Figure 4(a) showed the XRD patterns of the annealed $Sm_{1.1}Zr_{0.2}Fe_{9.2}Co_{2.3}Ti_{0.5}$ ribbons. Compared with the unannealed ones, the annealed ribbons exhibited peaks of α-Fe phase. Even if soft-magnetically α-Fe appears, the magnetic hardening has been achieved significantly, coercivity and remanence were greatly improved, as shown by the hysteresis loops (see Fig. S2(a)). With the increase of temperature, the coercivity monotonically increased, while the remanence first increased and then decreased, and the remanence ratio (larger than 0.5 after annealing) also increases and then decreases. At an annealing temperature of 850 °C, both remanence and remanence ratio reach their maximum values (Fig. 4(c)). Furthermore, the annealing time at 850 °C was regulated. The XRD patterns (Fig. 4(b)) revealed that the composition of annealed ribbons still consisted of a 1:12 main phase and a small amount α-Fe phase. The extension of annealing time did not cause significant changes of α-Fe content. In addition, as the annealing time prolonged, the coercivity gradually increased. And the remanence and remanence ratio both increased first and then decreased. It was worth noting that the optimal remanence ratio and remanence, saturation magnetization reached 0.61 emu/g and 86.1 emu/g, 141.1 emu/g, respectively, as shown in Figs. 4(c) and 4(d). It is worth mentioning again that after annealing, the diffraction peak of α-Fe appeared, but with the increase of annealing temperature and/or the extension of annealing time, the relative intensity of diffraction peaks of precipitated α-Fe did not increase. This phenomenon can be explained as a small amount of α-Fe precipitation after annealing, concomitantly, the remaining part transformed into a stable 1:12 phase structure. in other words, the supersaturated solid solution precipitated into a small amount α-Fe and stable 1:12 phase.

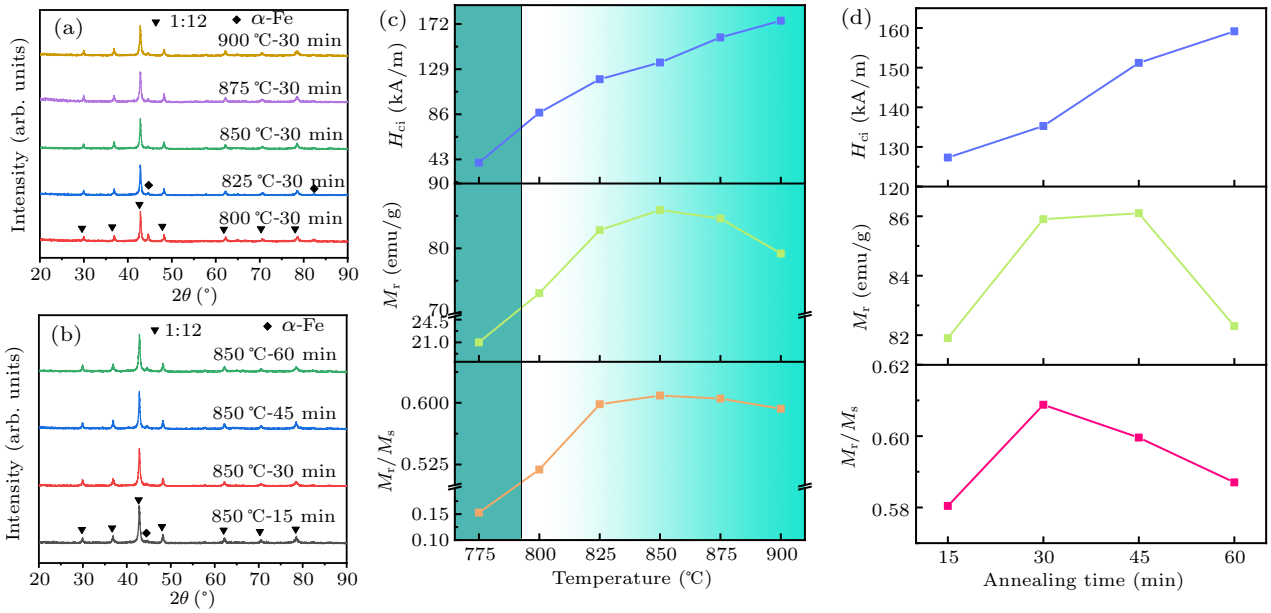


Fig. 4. Powdered XRD patterns [(a) and (b)] and magnetic properties [(c) and (d)] of the (Sm,Zr)(Fe,Co,Ti)$_{12}$ ribbons with different annealing temperatures [(a) and (c)] or with different annealing time [(b) and (d)].

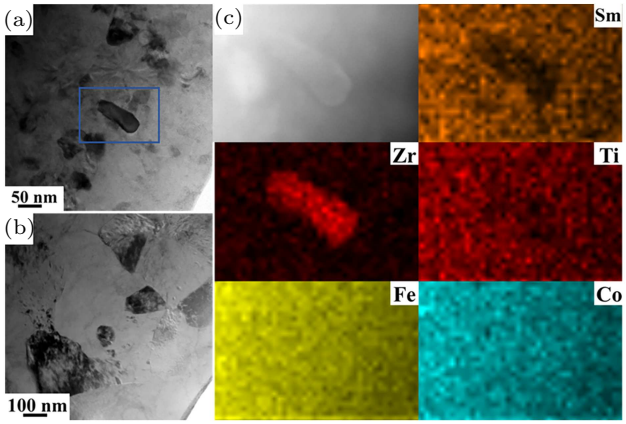


Fig. 5. TEM results of annealed (Sm,Zr)(Fe,Co,Ti)$_{12}$ ribbons at 850 °C and 45 min. Panels (a) and (b) are bright field images at different positions, panel (c) is HAADF image and *in-situ* distribution maps of Sm, Zr, Fe, Co, Ti elements of the position marked in panel (a).

Figure 5 showed the microstructure of the annealed ribbons. Compared with the fine-grain regions in the as-prepared ribbons (Fig. 3(a)), the grains significantly grew after annealing, however, coarse-grain regions (Figs. 3(b) and 5(b)) did not show significant growth before and after annealing. This also meant that the difference in grain size of the ribbons decreased after annealing, revealing the homogenization of microstructure. Note that the element segregation occurred after annealing. A small amount of Zr-rich and Sm-poor phases have precipitated, as shown in Fig. 5(c). In addition, the microstrain was obtained through geometric phase analysis by HRTEM, and the comparison showed that after annealing, the microstrain was significantly reduced. Figure 6 shows the HRTEM images and geometric phase analysis results before and after annealing. The corresponding FFT patterns from the HRTEM images showed that the ribbons both before and after annealing bearing a 1:12 phase structure, as shown in Figs. 6(a) and 6(b). The strain distribution obtained from the same crystallographic direction, as marked in the insets of Figs. 6(a) and 6(b), showed that the microstrain basically disappeared after annealing. Based on this, it can be inferred that after annealing, the supersaturated solid solution undergone grain size homogenization, α-Fe phase precipitation and Sm–Zr element segregation, and strain release. These factors should also be the reasons for achieving magnetic hardening, increase of remanence and coercivity.

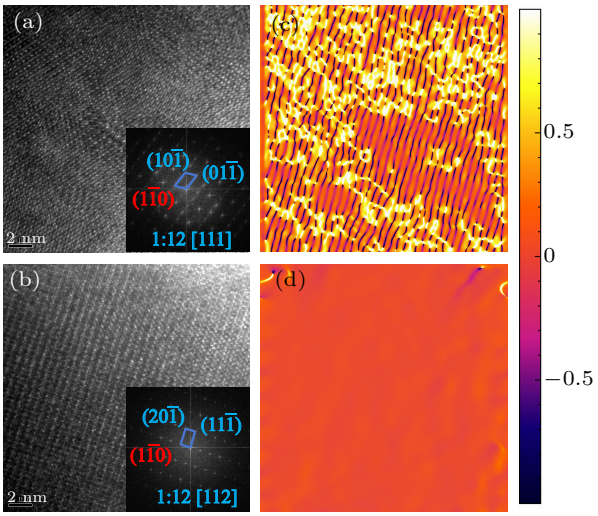


Fig. 6. HRTEM [(a) and (b)] images and corresponding geometric phase analysis results [(c) and (d)]. The insets in panels (a) and (b) showing the FFT patterns of corresponding HRTEM.

In addition, bulk nanocrystalline $Sm_{1.1}Zr_{0.2}Fe_{9.2}Co_{2.3}Ti_{0.5}$ magnets were also prepared using as-quenched ribbons as raw materials. The XRD result (Fig. 7(a)) showed that the magnet was mainly composed of a 1:12 phase and still a small amount

of α-Fe phase. The magnetic properties (Fig. 7(b)) were M_s (3 T) of 12.61 kGs, remanence of 4.02 kGs and coercivity of 1.12 kOe. The SEM results (Fig. 7(c)) revealed that There were two sources of α-Fe phase. One was the appearance of α-Fe aggregation in the powder contact area with high temperature caused by the discharge of the powder tip during the SPS process. Another was that a small portion of the ribbons had precipitated α-Fe. Large-sized α-Fe regions were the main reason for its low remanence and coercivity, revealing that the SPS should not be the optimal choice for preparing nanocrystalline magnets from the 1:12 quinary-alloy melt-spun ribbons.

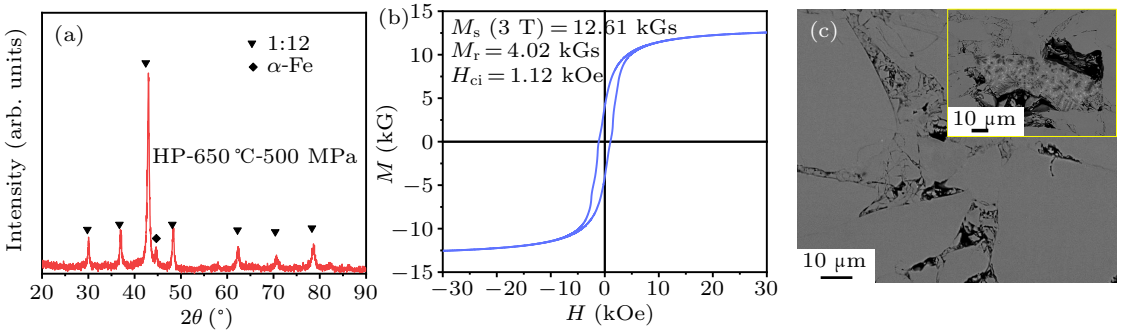


Fig. 7. XRD patterns, hysteresis loops (b), and SEM–BSE images (c) of the (Sm,Zr)(Fe,Co,Ti)$_{12}$ hot-pressed magnet.

4. Conclusion

This article showed that for low Ti content (Sm,Zr)(Fe,Co,Ti)$_{12}$ alloys, a 1:12 single-phase can be obtained through non-equilibrium pathways, but magnetic hardening cannot be achieved. After annealing, the supersaturated solid solution undergone grain size homogenization and Sm–Zr element segregation, and strain release, thus, increasing the remanence and coercivity, but the precipitation of α-Fe phase reducing coercivity. Our results can provide reference for exploring practical permanent magnets made of 1:12 type quinary-alloys.

Acknowledgements

Project supported by the National Key Research and Development Program of China (Grant No. 2021YFB3500300), the National Natural Science Foundation of China (Grant No. 51931007), and the Program of Top Disciplines Construction in Beijing (Grant No. PXM2019_014204_500031).

References

[1] Narasimhan K S V L 1981 *J. Appl. Phys.* **52** 2512
[2] Matsuura Y 2006 *J. Magn. Magn. Mater.* **303** 344
[3] Zhang X Y 2020 *Mater. Res. Lett.* **8** 49
[4] Li X H, Lou L and Song W P 2017 *Adv. Mater.* **29** 1606430
[5] Li X H, Lou L and Song W P 2017 *Nano Lett.* **17** 2985
[6] Li H L, Li X H and Guo D F 2016 *Nano Lett.* **16** 5631
[7] Teng Y, Li Y Q and Xu X C 2023 *J. Mater. Sci. Technol.* **138** 193
[8] Liu Y G, Xu L and Guo D F 2009 *J. Appl. Phys.* **106** 113918
[9] Poudel B, Amiri E and Rastgoufard P 2021 *IEEE Trans. Magn.* **57** 1
[10] Yang Y C, Kebe B and James W J 1981 *J. Appl. Phys.* **52** 2077
[11] Ohashi K, Tawara Y and Osugi R 1988 *J. Appl. Phys.* **64** 5714
[12] Gabay A M and Hadjipanayis G C 2017 *J. Magn. Magn. Mater.* **422** 43
[13] Tozman P, Sepehri-Amin H and Abe T 2023 *Acta Mater.* **258** 119197
[14] Matsumoto M, Hawai T and Ono K 2020 *Phys. Rev. Appl.* **13** 064028
[15] Chai W X, Huang Y L and Li H F 2024 *J. Mater. Res. Technol.* **29** 4676
[16] Ryzhikhin I, Andreev S and Semkin M 2019 *J. Phys. Conf. Ser.* **1389** 012117
[17] Kobayashi K, Suzuki S and Kuno T 2017 *J. Alloys Compd.* **694** 914
[18] Tozman P, Sepehri-Amin H and Takahashi Y K 2018 *Acta Mater.* **153** 354
[19] Yang Y C, Kong L S and Zha Y B 1988 *Le Journal de Physique Colloques* **49** 543
[20] Hu B P, Li H S and Gavigan J P 1989 *J. Phys.: Condens. Matter* **1** 755
[21] Tozman P, Sepehri-Amin H and Ohkubo T 2021 *J. Alloys Compd.* **855** 157491
[22] Hagiwara M, Sanada N and Sakurada S 2018 *J. Magn. Magn. Mater.* **465** 554
[23] Rong C B and Shen B G 2018 *Chin. Phys. B* **27** 117502
[24] Dirba I, Harashima Y and Sepehri-Amin H 2020 *J. Alloys Compd.* **813** 152224
[25] Zhang J S, Tang X and Sepehri-Amin H 2021 *Acta Mater.* **217** 117161
[26] Kuno T, Suzuki S and Urushibata K 2019 *Mater. Trans.* **60** 1697
[27] Zhao L Z, Li C L and Zhang X F 2020 *J. Alloys Compd.* **828** 154428
[28] Li Y C, Yu N J and Wu Q 2022 *J. Magn. Magn. Mater.* **549** 169065
[29] Neznakhin D S, Andreev S V and Semkin M A 2019 *J. Magn. Magn. Mater.* **484** 212
[30] Popov A G, Protasov A V and Gaviko V S 2019 *J. Rare Earths* **37** 1066
[31] Hÿtch M J, Snoeck E and Kilaas R 1998 *Ultramicroscopy* **74** 131